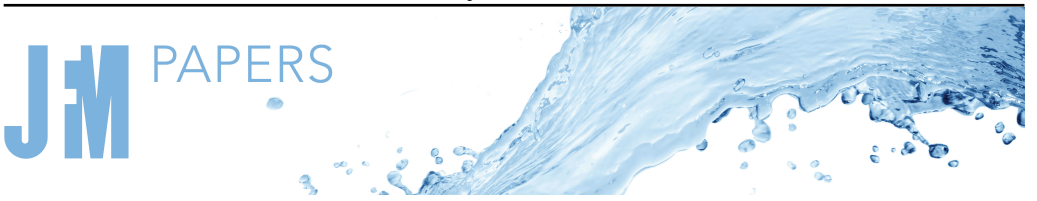
J. Fluid Mech. (2025), *vol.* 1008, A40, doi:10.1017/jfm.2025.232



Chemically active particles in extensional flow

Rahul Roy[1] **and Shubhadeep Mandal**[1]

[1]Department of Mechanical Engineering, Indian Institute of Science, Bengaluru 560012, India

Corresponding author: Shubhadeep Mandal, smandal@iisc.ac.in

(Received 21 August 2024; revised 6 February 2025; accepted 24 February 2025)

In a quiescent medium, chemically active particles propel themselves by emitting or absorbing solutes, creating concentration gradients that induce a slip at the particle surface. This self-propulsion occurs when solute advection overcomes diffusion. However, an imposed flow field can alter these dynamics. This study explores the propulsion characteristics and the related rheological consequences of chemically active particles in an imposed uniaxial extensional flow analytically and numerically. An asymptotic solution is obtained for weak imposed flow relative to self-induced diffusiophoretic slip. Meanwhile, finite element simulations are carried out over a wide range of imposed flow strength and Péclet number. The results reveal that the interplay between solute advection, imposed flow and diffusiophoretic slip significantly affects particle propulsion and suspension rheology. While solute advection and diffusiophoretic slip tend to create asymmetric solute distributions, promoting self-propulsion, imposed extensional flow promotes symmetric distributions, hindering self-propulsion. This not only delays the start of self-propulsion but also results in an early transition from a propulsion state to a stationary state characterised by an abrupt halt at relatively lower Péclet number compared to a quiescent medium. Post the abrupt halt, a stirring effect induced by particle activity and imposed extensional flow results in an increased magnitude of stresslet, thus a sudden change in the effective viscosity of the active suspension. The effect of imposed extensional flow on active particle dynamics and suspension rheology can be described succinctly by categorising the overall dynamics into three separate regimes, determined by the Péclet number and the intensity of the extensional flow.

Key words: microfluidics, swimming/flying

1. Introduction

Colloidal particles that have the ability to move on their own by carrying out interfacial physico-chemical interactions with the suspension medium are referred to as chemically active particles (Zöttl & Stark 2016; Illien, Golestanian & Sen 2017; Moran & Posner 2017;

© The Author(s), 2025. Published by Cambridge University Press. This is an Open Access article, distributed under the terms of the Creative Commons Attribution licence (https://creativecommons.org/licenses/by/4.0/), which permits unrestricted re-use, distribution and reproduction, provided the original article is properly cited.

https://doi.org/10.1017/jfm.2025.232 Published online by Cambridge University Press

Chen, Zhou & Wang 2019; Popescu 2020; Michelin 2023). The interfacial physico-chemical interaction results in the formation of a solute cloud around the colloid. This can lead to the motion of the particle if the solute cloud is distributed asymmetrically at the particle surface (Ramaswamy 2010; Michelin, Lauga & Bartolo 2013; Illien *et al.* 2017; Farutin *et al.* 2023). The asymmetry is achieved by default in active particles that are chemically asymmetric, known as Janus particles (Golestanian, Liverpool & Ajdari 2007; Howse *et al.* 2007; Ebbens & Howse 2010; Zhao & Pumera 2012). For chemically isotropic particles, the asymmetric solute cloud is achieved through a symmetry-breaking instability caused by advection of solute (Michelin *et al.* 2013; Hu *et al.* 2019; Saha, Yariv & Schnitzer 2021; Kailasham & Khair 2022; Saha & Yariv 2022). Potentially, these active particles could be used in various applications, such as micromixing, microscale cargo transport, drug delivery, and more (Wirtz 2009; Wang 2013; Maass *et al.* 2016; Saintillan 2018; Kailasham & Khair 2023*a*; Yang *et al.* 2024). The presence of a flow field, either internally induced and/or externally imposed, is inevitable in most applications (Saintillan 2018; Saha *et al.* 2021; Kailasham & Khair 2022; Picella & Michelin 2022). The interaction between the moving particles and the induced or imposed flow field often leads to interesting motion of active particles and unusual rheological properties of the active suspension (Frankel & Khair 2014; Ten Hagen *et al.* 2014; Uspal *et al.* 2015; Stark 2016; Katuri *et al.* 2018; Brosseau *et al.* 2019; Si, Patel & Mangal 2020; Sharan *et al.* 2022), necessitating additional investigation.

The phenomenon of self-propulsion even in the absence of any external force or flow is the hallmark of a chemically active particle (Michelin *et al.* 2013; Michelin & Lauga 2014). This has been established by theoretical as well as experimental observation on active droplets such that the active particle serves as a model for active droplets (Izri *et al.* 2014; Maass *et al.* 2016; Seemann, Fleury & Maass 2016; Morozov & Michelin 2019*b*; Michelin 2023; Chen *et al.* 2024). Here, we focus on chemically active particles, which are chemically and geometrically isotropic. The spontaneous motion of such particles is caused by an uneven distribution of solute concentration over their surface. The asymmetry in solute concentration is linked to two important characteristics: (i) surface activity, which refers to the interchange of solute with the surrounding medium, and (ii) mobility, which represents the interactions that turn solute concentration gradients into diffusiophoretic slip across short distances (Michelin *et al.* 2013; Yariv & Kaynan 2017; Saha *et al.* 2021). The initial perturbations in solute distribution over the particle surface caused by the interfacial chemical interaction are enhanced by the diffusiophoretic slip. The particle will start moving only if the solute advection due to diffusiophoretic slip is sufficiently strong to counter the homogenising effects of diffusion. The self-propulsion of the active particles is therefore quantified using the Péclet number Pe, which allows for the characterisation of different instability modes in the particle's behaviour (Chen *et al.* 2021; Desai & Michelin 2021; Hokmabad *et al.* 2021; Kailasham & Khair 2022). The self-propulsion starts after the advent of the first instability mode at threshold value $Pe = 4$, which indicates the breaking of the symmetry of the solute cloud around the particle surface (Michelin *et al.* 2013; Chen *et al.* 2021; Kailasham & Khair 2022). The particle's self-propulsion creates a disturbance in the surrounding medium, which results in the production of an active stresslet in the suspension (Lauga & Michelin 2016; Saintillan 2018). As a result, the suspension's effective viscosity and rheological properties are also altered. This continues until the higher-order instability surpasses the first-order instability. When the Péclet number Pe exceeds 26, the higher-order instability becomes more dominant than the first-order instability, causing the particle to stop abruptly (Morozov & Michelin 2019*a*; Kailasham & Khair 2022). This is characterised by a symmetric solute cloud around the particle with the flow field resembling a straining flow (Kailasham & Khair 2022).

https://doi.org/10.1017/jfm.2025.232 Published online by Cambridge University Press

On increasing the Péclet number ($Pe \geqslant 55$) even further, the particle exhibits a short burst of self-propulsion characterised by a sharp and random change in both the speed and direction of motion. This is referred to as a chaotic regime (Hu *et al.* 2019; Kailasham & Khair 2022). Theoretical investigation of the instability associated with the near-threshold Pe (e.g. $Pe = 4$ for the onset of self-propulsion) is quite challenging. In this regard, Schnitzer (2023) and Peng & Schnitzer (2023), in their series of weakly nonlinear dynamics of active particles, have presented the first unsteady and fully three-dimensional weakly nonlinear perturbation approach to study the onset of spontaneous dynamics of active particles, including perturbation effects such as external forces and torques.

In addition to the internally induced flow, the active particles are often subjected to an external force or flow field (Frankel & Khair 2014; Saintillan 2018; Saha *et al.* 2021; Kailasham & Khair 2023*b*; Peng & Schnitzer 2023; Schnitzer 2023). Linear flows – which includes shear and extensional flows – are commonly encountered in microscale processes. Although it has been observed that imposed shear flow significantly impacts the overall behaviour and rheology of active suspensions (Frankel & Khair 2014; Saintillan 2018; Kailasham & Khair 2023*b*), only a handful of studies in the literature explore the coupled effect of particle surface activity and an imposed linear flow field. The rheology of active particle suspension exhibits a transition from chaotic to periodic to eventually steady rheology with an increase in shear strain rate (Kailasham & Khair 2023*b*). The effective viscosity of active biological suspension in the presence of an imposed shear flow either increases or decreases depending upon the active motion of the biological swimmer (Koch & Subramanian 2011; Saintillan 2018). For a pusher-type extensile motion (*E.coli*), the active stresslet tends to reduce the effective viscosity, whereas a contractile puller-type motion (*C. reinhardtii*) results in an active flow opposing the imposed shear, thereby increasing the effective viscosity of the suspension (Saintillan 2010). It is also observed that with the increase in motility, the extensional viscosity of suspension of algal pullers increases, whereas the extensional viscosity decreases for bacterial or sperm pushers (McDonnell *et al.* 2015). Thus the coupled effect of imposed extensional flow and particle surface activity on a particle's propulsion characteristics and effective suspension rheology will provide a deeper understanding of the underlying biophysical phenomena as well as providing insights into applications associated with engineered active suspensions.

Motivated by these concerns, here we carry out an investigation to explore the combined effect of imposed uniaxial extensional flow and particle activity on its self-propulsion characteristics and its impact on suspension rheology. At first, it is explored from a theoretical viewpoint, which is valid for weak extensional flow and away from the instability threshold. For moderate and strong extensional flow, the investigation was performed numerically after its theoretical validation at a weak extensional flow. We also obtain various regimes depicting the resulting propulsion characteristic and overall fluid rheology as function of Péclet number and the strength of imposed extensional flow.

2. Mathematical modelling

The objective of the present study is to analyse the motion of an active particle and its impact on suspension rheology when subjected to an imposed uniaxial extensional flow. We will focus on the nonlinear coupling between chemical transport in the bulk fluid, solute emission at the particle surface, and the flow of fluid driven by the self-generated diffusiophoretic velocity, which will determine the motion of particles and the rheology of the suspension. Since it is a common practice to study single-particle dynamics to obtain rheological effects on dilute suspensions (Taylor 1932; Lin, Peery & Schowalter 1970; Raja, Subramanian & Koch 2010; Subramanian *et al.* 2011; Lauga & Michelin

https://doi.org/10.1017/jfm.2025.232 Published online by Cambridge University Press

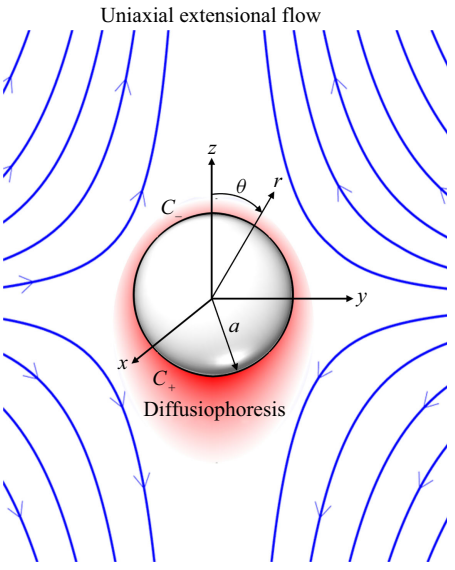


Figure 1. An active particle with diffusiophoretic slip denoted by $C_+ > C_-$ encountering a uniaxial extensional flow $\boldsymbol{u}_\infty$, where C denotes the solute concentration. The asymmetric solute cloud around the particle surface due to surface activity, diffusiophoresis and advection results in self-propulsion of the particle.

2016; Mandal *et al.* 2018; Saintillan 2018), the present study will focus on single-particle dynamics to obtain crucial insights into the rheological behaviour of dilute suspensions.

2.1. *Physical system*

A chemically isotropic active spherical particle of radius a is suspended in an unbounded fluid with solute concentration C and subjected to an imposed uniaxial extensional flow as shown in figure 1. The far-field velocity $\boldsymbol{u}_\infty$ is the velocity field associated with the imposed uniaxial extensional flow. For extensional flow, the velocity field is expressed as $\boldsymbol{u}_\infty = \boldsymbol{\Gamma} \cdot \boldsymbol{x}$, where $\boldsymbol{x}$ is the position vector, and $\boldsymbol{\Gamma}$ represents the rate-of-strain tensor. This imposed extensional flow is symmetric in nature, with the corresponding velocity scale represented by Ga, where G is the strain rate of the extensional flow. The rate-of-strain tensor for uniaxial extensional flow is of the form

$$\boldsymbol{\Gamma} = \frac{G}{2}\begin{bmatrix} -1 & 0 & 0 \\ 0 & -1 & 0 \\ 0 & 0 & 2 \end{bmatrix}. \tag{2.1}$$

The interfacial activity at the particle surface, represented by $\mathcal{A}$, results in a formation of excess solute cloud near the particle surface such that the difference between local concentration and far-field solute concentration C_∞ is of the order $\mathcal{C} = |\mathcal{A}|\, a/\mathcal{D}$, where $\mathcal{D}$ represents the solute diffusivity. This interfacial gradient of solute concentration coupled with mobility results in the formation of diffusiophoretic slip, such that the velocity scale corresponding to the slip is expressed as $\mathcal{U} = |\mathcal{A}\mathcal{M}|/\mathcal{D}$, where $\mathcal{M}$ is the mobility parameter (Michelin *et al.* 2013; Saha *et al.* 2021). Thus the corresponding Péclet number quantifying the solute advection relative to diffusion is expressed as $Pe = \mathcal{U}a/\mathcal{D} = |\mathcal{A}\mathcal{M}|\, a/\mathcal{D}^2$.

For analytical simplification, all equations have been normalised. Consequently, the remainder of the paper employs dimensionless variables unless explicitly stated otherwise. By normalising length variables by a, solute concentration by $\mathcal{C}$, velocity by $\mathcal{U}$, and time by

https://doi.org/10.1017/jfm.2025.232 Published online by Cambridge University Press

$a/\mathcal{U}$, the non-dimensional form of the advection–diffusion equation, governing the excess solute concentration distribution, is expressed as

$$Pe\left(\frac{\partial C}{\partial t}+\boldsymbol{u}\cdot\boldsymbol{\nabla}C\right)=\nabla^2 C. \tag{2.2}$$

The advection term in this equation illustrates the nonlinear coupling between the solute concentration and the velocity field. The isotropic surface flux condition is represented as

$$\left.\frac{\partial C}{\partial r}\right|_{r=1}=-A, \tag{2.3}$$

where $A=\mathcal{A}/|\mathcal{A}|=\pm 1$ is dimensionless activity. The far-field attenuation condition is represented as

$$C|_{r\to\infty}\to 0. \tag{2.4}$$

The fluid flow is governed by the continuity and Navier–Stokes equations as

$$\boldsymbol{\nabla}\cdot\boldsymbol{u}=0,\quad Re\left(\frac{\partial \boldsymbol{u}}{\partial t}+\boldsymbol{u}\cdot\boldsymbol{\nabla}\boldsymbol{u}\right)=-\boldsymbol{\nabla}p+\nabla^2\boldsymbol{u}, \tag{2.5}$$

where the pressure is non-dimensionalised by $\mu\mathcal{U}/a$, and $Re=\rho a\mathcal{U}/\mu$ is the Reynolds number, with ρ being the fluid density, and μ being the fluid viscosity.

At the particle surface, the diffusiophoretic slip is characterised as

$$\boldsymbol{u}|_{r=1}=M\,\boldsymbol{\nabla}_s C, \tag{2.6}$$

where $\boldsymbol{\nabla}_s=(\boldsymbol{I}-\boldsymbol{nn})\cdot\boldsymbol{\nabla}$ represents surface gradient operator, and $M=\mathcal{M}/|\mathcal{M}|=\pm 1$ is the dimensionless mobility. This surface slip condition couples the flow field with the solute concentration. With the reference frame moving with the particle, the flow field as $r\to\infty$ could be represented as

$$\boldsymbol{u}_\infty\to\frac{\epsilon}{2}\begin{bmatrix}-1&0&0\\0&-1&0\\0&0&2\end{bmatrix}\cdot\boldsymbol{x}-\boldsymbol{U}, \tag{2.7}$$

where $\boldsymbol{U}$ represents the particle velocity. The dimensionless extension rate is given by $\epsilon=Ga/\mathcal{U}$, which represents the ratio of the velocity scales due to imposed uniaxial extensional flow and diffusiophoresis. Thus ϵ is a measure of the strength of imposed extensional flow. The particle velocity is governed by the Newton's second law of motion:

$$\frac{d\boldsymbol{U}}{dt}=\int_{A_p}(\boldsymbol{\sigma}\cdot\boldsymbol{n})\,dA, \tag{2.8}$$

where $\boldsymbol{\sigma}=-p\boldsymbol{I}+\boldsymbol{\nabla}\boldsymbol{u}+(\boldsymbol{\nabla}\boldsymbol{u})^T$ is the hydrodynamic stress tensor, A_p is the particle surface, and $\boldsymbol{n}$ is the outward unit normal on A_p. The right-hand side of (2.8) represents the total hydrodynamic force on the particle. At the steady state, the total hydrodynamic force vanishes, and the particle translates in a force-free manner.

The motion of particles in a suspension alters the overall suspension rheology due to the disturbance flow generated by individual particles that interact with external flows, impacting the rheological characteristics of the suspension. The stresslet accounts for the stress due to individual particles to the bulk fluid stress. For dilute suspension with low volume fraction such that the particle–particle hydrodynamic interaction is absent (or negligible), the effective suspension rheology is dependent directly on the stresslet and

https://doi.org/10.1017/jfm.2025.232 Published online by Cambridge University Press

the volume fraction. In the present study, the stresslet $\boldsymbol{S}$ is determined using the following expression derived by Batchelor (1970) for a particle:

$$\boldsymbol{S} = \int_{A_p} \left[\tfrac{1}{2} \left\{ (\boldsymbol{\sigma} \cdot \boldsymbol{n})\, \boldsymbol{x} + ((\boldsymbol{\sigma} \cdot \boldsymbol{n})\, \boldsymbol{x})^T - \tfrac{2}{3} \boldsymbol{I}\, (\boldsymbol{\sigma} \cdot \boldsymbol{n}) \cdot \boldsymbol{x} \right\} - \left(\boldsymbol{u}\boldsymbol{n} + (\boldsymbol{u}\boldsymbol{n})^T \right) \right] dA. \quad (2.9)$$

Before discussing the asymptotic and numerical approach for solving the nonlinear particle dynamics, it is important to note that the coupled problem involving an active particle and imposed extensional flow will now depend on Pe as well as ϵ. This coupled and nonlinear nature of the mathematical model cannot be directly solved analytically for arbitrary Pe and ϵ.

2.2. *Asymptotic solution*

We obtain the analytical solution based on the following key assumptions. (i) The flow and chemical transport are axisymmetric, and the particle stays very close to the stagnation point of the imposed extensional flow. (ii) The fluid inertia is negligible compared to the viscous effects. (iii) Steady state is assumed. (iv) There is small ϵ linearisation about the stationary base state and away from any bifurcations (i.e. $Pe < 4$).

The asymptotic steady-state solution is obtained for motion of the active particle in the limit of negligible fluid inertia, $Re \ll 1$. In this limit, the governing equation for fluid flow (2.5) and solute concentration distribution (2.2) can be rewritten as

$$\boldsymbol{\nabla} \cdot \boldsymbol{u} = 0, \quad -\boldsymbol{\nabla} p + \nabla^2 \boldsymbol{u} = \boldsymbol{0}, \quad (2.10)$$

$$Pe\, \boldsymbol{u} \cdot \boldsymbol{\nabla} C = \nabla^2 C. \quad (2.11)$$

In the limit $\epsilon \ll 1$, the asymptotic expansion for any dependent variable (e.g. solute concentration C) is of the form

$$C = C^{(0)} + \epsilon C^{(1)} + \epsilon^2 C^{(2)} + \cdots . \quad (2.12)$$

This is such that the leading order or the base state corresponds to a trivial solution with no flow and a spherically symmetric source distribution for solute concentration around a stationary particle, represented as

$$\boldsymbol{u}^{(0)} = \boldsymbol{0}, \quad U^{(0)} = 0, \quad C^{(0)} = \frac{A}{r}. \quad (2.13)$$

Considering the axial symmetry of fluid flow and chemical transport, we have chosen an axisymmetric spherical coordinate system (r, θ). For an asymptotically small value of ϵ, the perturbation expansion represents the $O(\epsilon)$ deviation from the base state of spherical symmetry. Considering the axisymmetric nature of the flow field, the fluid flow is expressed through stream function $\psi^{(1)}$, such that the radial and tangential velocity components can be expressed as

$$u_r^{(1)} = -\frac{1}{r^2} \frac{\partial \psi^{(1)}}{\partial \eta} \quad \text{and} \quad u_\theta^{(1)} = -\frac{1}{r\sqrt{1-\eta^2}} \frac{\partial \psi^{(1)}}{\partial r}, \quad (2.14)$$

where $\eta = \cos\theta$. The Stokes equation (2.5) can thus be expressed as (Leal 2007)

$$E^4 \psi^{(1)} = 0, \quad (2.15)$$

where $E^2 \equiv \frac{\partial^2}{\partial r^2} - \frac{(1-\eta^2)}{r^2} \frac{\partial^2}{\partial \eta^2}$. Using the stream function leads to satisfaction of the continuity equation automatically, while the solution of the Stokes equation (2.15) yields a

https://doi.org/10.1017/jfm.2025.232 Published online by Cambridge University Press

generalised expression of the stream function for a particle in an axisymmetric flow field, where the stream function can be expressed as (Leal 2007)

$$\psi^{(1)} = \sum_{n=1}^{\infty} \left[\mathsf{A}_n r^{n+3} + \mathsf{B}_n r^{n+1} + \mathsf{E}_n r^{2-n} + \mathsf{F}_n r^{-n} \right] Q_n(\eta), \tag{2.16}$$

where $Q_n(\eta)$ is the Gegenbauer polynomial. The $O(\epsilon)$ far-field flow velocity from (2.7) becomes

$$\boldsymbol{u}_\infty^{(1)} \to \frac{r}{2} \left[\left(3\eta^2 - 1 - \frac{2U^{(1)}}{r}\eta \right) \boldsymbol{e}_r \; - \left(3\eta\sqrt{1-\eta^2} - \frac{2U^{(1)}}{r}\sqrt{1-\eta^2} \right) \boldsymbol{e}_\theta \right], \tag{2.17}$$

where $\boldsymbol{e}_r$ and $\boldsymbol{e}_\theta$ are unit vectors in spherical coordinates, with $U^{(1)}$ being the $O(\epsilon)$ particle velocity. Applying the far-field condition on the stream function, the values of the constants can be determined as

$$\begin{aligned} &\mathsf{A}_n = 0 \text{ for } n \geqslant 1, \\ &\mathsf{B}_n = 0 \text{ for } n \geqslant 2, \\ &\mathsf{B}_1 = U^{(1)} \text{ and } \mathsf{B}_2 = -1. \end{aligned} \tag{2.18}$$

Thus the stream function is of the form

$$\psi^{(1)} = U^{(1)} r^2 \, Q_1(\eta) - r^3 \, Q_2(\eta) + \sum_{n=1}^{\infty} \left[\mathsf{E}_n r^{2-n} + \mathsf{F}_n r^{-n} \right] Q_n(\eta). \tag{2.19}$$

The far-field stream function includes $Q_1(\eta)$ and $Q_2(\eta)$, therefore by considering $n = 1$ and $n = 2$, the respective stream function is

$$\psi^{(1)} = \left(U^{(1)} r^2 + \frac{\mathsf{F}_1}{r} + \mathsf{E}_1 r \right) Q_1(\eta) + \left(-r^3 + \mathsf{E}_2 + \frac{\mathsf{F}_2}{r^2} \right) Q_2(\eta). \tag{2.20}$$

By incorporating a no-penetration boundary condition at the particle surface, i.e. $u_r|_{r=1} = 0$, we get $\mathsf{E}_1 + \mathsf{F}_1 + U^{(1)} = 0$ and $\mathsf{E}_2 + \mathsf{F}_2 = 1$. Substituting E_2 in terms of F_2, the stream function takes the form

$$\psi^{(1)} = \left[U^{(1)} r^2 + \frac{\mathsf{F}_1}{r} + \mathsf{E}_1 r \right] Q_1(\eta) + \left[-r^3 + 1 + \mathsf{F}_2 \left(\frac{1}{r^2} - 1 \right) \right] Q_2(\eta). \tag{2.21}$$

The $O(1)$ and $O(\epsilon)$ solute transport equations are respectively of the form

$$\nabla^2 C^{(0)} = 0 \quad \text{for } O(1), \tag{2.22}$$

$$\nabla^2 C^{(1)} = Pe \, \boldsymbol{u}^{(1)} \cdot \nabla C^{(0)} \quad \text{for } O(\epsilon), \tag{2.23}$$

such that $(\partial C^{(0)}/\partial r)|_{r=1} = -A$, $(\partial C^{(1)}/\partial r)|_{r=1} = 0$ and $C^{(0)}|_{r\to\infty} = C^{(1)}|_{r\to\infty} = 0$. On applying the boundary conditions, the final expression for the $O(\epsilon)$ solute transport equation is of the form

$$\nabla^2 C^{(1)} = Pe \; A \left[\left\{ \frac{U^{(1)}}{r^2} + \frac{\mathsf{F}_1}{r^5} + \frac{\mathsf{E}_1}{r^3} \right\} P_1(\eta) - \left\{ \frac{1}{r} - \frac{1}{r^4} - \mathsf{F}_2 \left(\frac{1}{r^6} - \frac{1}{r^4} \right) \right\} P_2(\eta) \right], \tag{2.24}$$

https://doi.org/10.1017/jfm.2025.232 Published online by Cambridge University Press

where $P_n(\eta)$ is the Legendre polynomial of degree n. By solving this equation, the solute concentration is found to be of the form

$$C^{(1)} = -Pe\,A\left[\frac{U^{(1)}}{2} - \frac{\mathsf{F}_1}{4r^3} + \frac{\mathsf{E}_1}{2r} + \frac{1}{r^2}\left(\frac{3\mathsf{F}_1}{8} - \frac{\mathsf{E}_1}{4}\right)\right]P_1(\eta) - Pe\,A\left[-\frac{r}{4} - \frac{\mathsf{F}_2}{6r^4} + \frac{1}{r^2}\left(-\frac{\mathsf{F}_2}{4} + \frac{1}{4}\right) + \frac{1}{r^3}\left(-\frac{1}{4} + \frac{7\mathsf{F}_2}{18}\right)\right]P_2(\eta). \tag{2.25}$$

The diffusiophoretic slip at the particle surface corresponds to $u_\theta|_{r=1} = -M\sqrt{1-\eta^2}(\partial C^{(1)}/\partial\eta)|_{r=1}$. After substituting the expressions of solute concentration in the expression obtained from the slip condition , i.e.

$$\frac{\mathsf{F}_1 - 2U^{(1)} - \mathsf{E}_1}{2} + \frac{(3+2\mathsf{F}_2)\eta}{2} = M\left.\frac{\partial C^{(1)}}{\partial\eta}\right|_{r=1}, \tag{2.26}$$

one can determine the value of the unknown constants E_1 and F_2 as

$$\mathsf{E}_1 = U^{(1)}\left(\frac{12 - 3AM\,Pe}{AM\,Pe - 8}\right), \tag{2.27}$$

$$\mathsf{F}_2 = \frac{9\,(-2 + AM\,Pe)}{12 - AM\,Pe} = -\frac{3}{2} + 3C_2M. \tag{2.28}$$

For the force-free condition, $\mathsf{E}_1 = 0$, which implies that the particle velocity is $U^{(1)} = 0$ up to $O(\epsilon)$. Similar results have been obtained in the studies carried out by Michelin *et al.* (2013) and Saha *et al.* (2021). Also, it is important to note that away from bifurcation, the particle is motionless even in the presence of extensional flow due to symmetry of the flow. Here, C_2 is the coefficient of the second-degree Legendre polynomial when the solute concentration distribution on the particle surface is expressed in terms of Legendre polynomials as

$$C|_{r=1} = \sum_{n=0}^{\infty} C_n\,P_n(\eta). \tag{2.29}$$

For large r, the above solution for $O(\epsilon)$ solute concentration does not satisfy the far-field condition. One can use matched asymptotic expansion to obtain the far-field correction, which has been done for a passive phoretic particle in linear flow at low Pe by Yariv & Kaynan (2017). Since the solute concentration at the particle surface is independent of the far-field solution, as shown by Saha *et al.* (2021) and Yariv & Kaynan (2017), the far-field solution has not been evaluated in the present study. However, the far-field solution can be obtained by applying the matched asymptotic solution, as followed by Saha *et al.* (2021).

For an axisymmetric particle self-propelling in direction $\boldsymbol{e}$ (z-direction), the stresslet tensor ($\boldsymbol{S}$) can be expressed in terms of a scalar stresslet intensity (S) as $\boldsymbol{S} = S(\boldsymbol{ee} - (1/3)\boldsymbol{I})$. The velocity field and the stress tensor are determined directly from the stream function, with an additional determination of fluid pressure through the Stokes equation to determine the diagonal elements of the stress tensor. This yields the stresslet intensity S up to $O(\epsilon)$ to be of the form

$$S = (10\pi - 12\pi C_2 M)\,\epsilon = 40\pi\left[1 - \frac{9}{12 - AM\;Pe}\right]\epsilon. \tag{2.30}$$

Stresslet intensity S indicates the effective viscosity of the suspension. A positive value of the stresslet represents the case of active particles showcasing puller-type motion,

https://doi.org/10.1017/jfm.2025.232 Published online by Cambridge University Press

thereby increasing the effective viscosity, whereas a negative value of the stresslet, on the other hand, represents the active particle behaving as a pusher, thereby decreasing the effective viscosity of the active suspension (Saintillan 2010, 2018; Lauga & Michelin 2016). A higher magnitude of S, irrespective of its sign, represents the impact of a particle in influencing the suspension rheology. It is important to note that the self-propulsion and stresslet depend on the sign of AM. Negative AM represents the scenario of no self-propulsion (Michelin *et al.* 2013), thus the suspension also behaves as a suspension of passive particles. The chemical transport for negative AM gives rise to a diffusiophoretic slip which resists the imposed extensional flow and thereby enhances the stresslet as represented in (2.30). On the other hand, positive AM represents a state of self-propulsion beyond the threshold $Pe = 4$ (Michelin *et al.* 2013). The chemical transport for positive AM gives rise to a diffusiophoretic slip that augments the imposed extensional flow and thereby reduces the stresslet as represented in (2.30). It is important to note that for positive AM, due to the first-order dipolar instability resulting in the particle self-propulsion, the assumed motionless isotropic base state is not valid for all values of Pe (Schnitzer 2023), thereby limiting the theoretical expression derived in (2.30) to be applicable for $Pe \leqslant 4$ only.

2.3. *Numerical solution*

In the case of an active particle in imposed uniaxial extensional flow, the asymptotic solution is applicable only when the imposed extensional flow is weak in comparison to the diffusiophoretic slip, i.e. ϵ is small. Also, for positive AM, due to the dipolar instability at $Pe = 4$, the perturbation solution (2.30) is limited to $Pe \leqslant 4$ only. In addition to this, the particle sets into motion due to instability of dipolar perturbation, and further increase in Pe results in instability of other types of perturbations (such as quadrupolar) (Hu *et al.* 2022; Kailasham & Khair 2022). To address these limitations, we carry out numerical analysis over a wide range of ϵ and Pe.

The particle velocity and stresslet intensity are obtained through numerical simulations of the governing equations (2.5) and (2.2) for fluid flow and solute concentration subject to boundary conditions (2.6), (2.7) and (2.3), (2.4), respectively, using the finite element-based simulation framework COMSOL Multiphysics (Zhu & Zhu 2023; Shreekrishna, Mandal & Das 2024). For simulations, an axisymmetric problem is solved with a spherical particle being at the stagnation point of the imposed extensional flow with unit radius in an axisymmetric computational domain (with non-dimensional size 50×100). To inculcate the effects of increasing Pe, along with the possibility of the presence of an initial asymmetry in the concentration distribution, the initial concentration field is expressed following Kailasham & Khair (2022) as

$$C|_{(r=1,t=0)} = \frac{A}{r} - \delta_{per}\left(\frac{\cos\theta}{r^2}\right), \tag{2.31}$$

with $|\delta_{per}| < 1$, such that initial asymmetry is inculcated with an axisymmetric concentration distribution. We chose the default triangular mesh element setting with linear elements for both the velocity components and the pressure field (P1 + P1). The element size is finer near the particle–fluid interface as compared to the fluid domain where the maximum element sizes 0.008 and 0.5 were used for meshing the particle surface and the fluid domain, respectively. The mesh sizes are selected based upon a convergence test performed with coarse mesh, fine mesh and very fine mesh, where the respective maximum element sizes of the fluid domain and the particle surface were 1, 0.05 (coarse mesh), 0.5, 0.008 (fine mesh), and 0.2, 0.002 (very fine mesh).

https://doi.org/10.1017/jfm.2025.232 Published online by Cambridge University Press

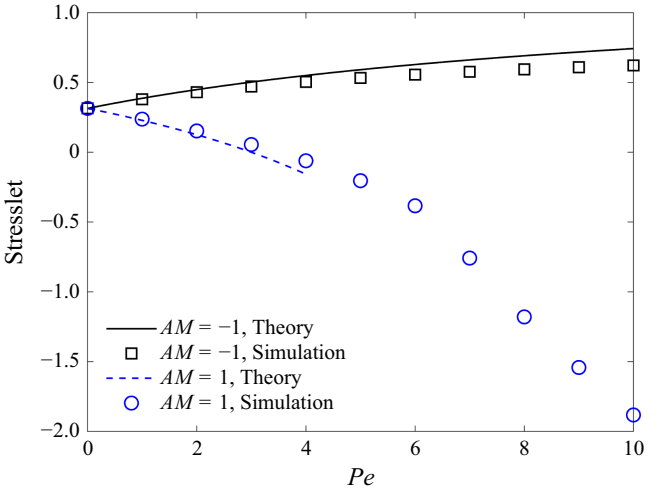


Figure 2. Theoretically and numerically obtained stresslet for a particle subjected to a weak uniaxial extensional flow with $\epsilon = 0.01$ and positive and negative values of AM.

The domain size 50×100 is selected post domain independence tests performed on three fluid domains of sizes 30×60, 50×100 and 60×120. The Navier–Stokes equation along with the continuity equation is solved in the computation model by using the 'laminar flow' interface. This is coupled with the 'stabilised convection–diffusion' equation to solve the solute concentration distribution with the application of a slip velocity at the particle surface. The Reynolds number for the fluid flow in the domain was kept at $Re = 0.01$. A time-dependent BDF solver with relative tolerance of 10^{-6} is used alongside a direct PARDISO solver.

The comparison between theoretical and numerical simulation is represented in figure 2. The theoretical and numerical simulations exhibit strong similarity for all values of Pe when $AM = -1$. However, for $AM = 1$, i.e. the case of self-propulsion, it can be observed that the theoretical and the numerical simulations are in close resemblance for $Pe \sim 4$, beyond which the theoretical results diverge due to instability, resulting in self-propulsion at $Pe = 4$. When $AM = -1$, the stresslet is observed to remain positive for all values of $Pe > 0$. This adheres to the fact that the effective viscosity of passive particle suspension is more than the background fluid viscosity. On the contrary, the stresslet changes sign after a particular value of Pe when $AM > 0$. In addition to this, the numerical simulations compare very well with the existing results for the case of active particles in a quiescent medium, as represented in figure 3. Thus numerical simulations are carried out to analyse active particle propulsion and the associated stresslet in the imposed uniaxial extensional flow condition.

3. Results and discussion

3.1. *Motion in a quiescent medium*

The motion of an active particle in the absence of any imposed flow is the sole consequence of the coupled effect of particle surface activity and the interfacial diffusiophoretic slip caused by the mobility. Depending upon the magnitude of the Péclet number, the solute concentration distribution across the particle surface is modified such that the active particle motion can be characterised by three distinct regimes, namely (i) quiescent, (ii) self-propulsion and (iii) stirring, as depicted in figure 3 (Michelin *et al.*

https://doi.org/10.1017/jfm.2025.232 Published online by Cambridge University Press

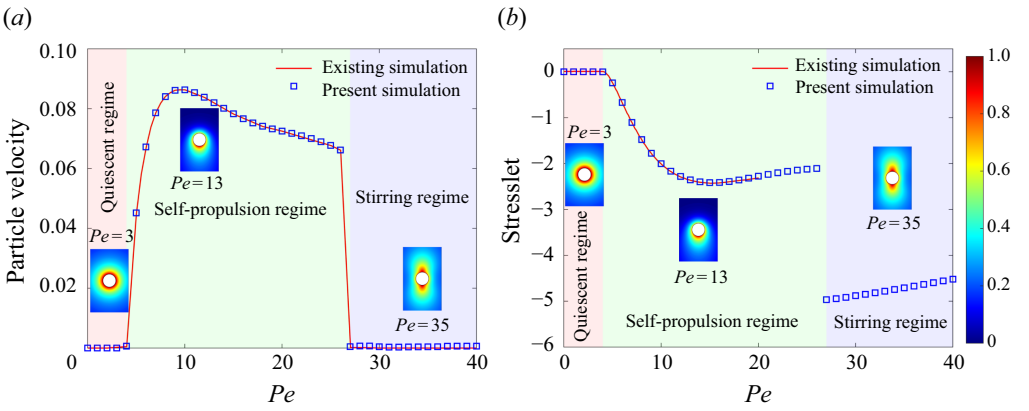


Figure 3. Motion of an active particle in the absence of any imposed background flow. The present numerical simulation is validated with results in the literature. Particle velocity is validated from Kailasham & Khair (2022) and Hu *et al.* (2022), and the stresslet is validated from Michelin *et al.* (2013). Plots show the variation of particle velocity and the induced stresslet with Péclet number for an active particle in the absence of any imposed flow. The surface plot shows qualitatively the symmetry breaking in the solute concentration around the particle surface.

2013; Hu *et al.* 2022; Kailasham & Khair 2022). At low values of the Péclet number, the solute advection over the particle surface is weak compared to the diffusive transport of solute. As a result, the solute cloud surrounding the particle remains symmetric, while the particle remains stationary. This is represented by the quiescent regime, which extends to a critical value of the Péclet number, above which the solute advection is strong enough to overcome the uniforming effects of diffusion. As a consequence, the symmetry in solute concentration distribution is broken once the Péclet number is greater than the critical Péclet number. Above this threshold Péclet number, the quiescent state becomes unstable, and spontaneous particle motion occurs under small perturbation. This threshold value of the Péclet number representing the onset of self-propulsion is denoted by Pe_1, which is found to be $Pe_1 = 4$. This symmetry breaking is characterised by the onset of particle motion, i.e. self-propulsion. This is associated with the onset of the first hydrodynamic instability mode, which is also referred to as dipolar instability (Hokmabad *et al.* 2021). The insets showing the surface plot in figure 3(*a*) depict the symmetry breaking in solute distribution. The self-propulsion regime continues until the Péclet number attains a critical value $Pe_2 \approx 27$ (Kailasham & Khair 2022). This Pe_2 denotes the critical value of the Péclet number for the transition from self-propulsion to the stirring regime. The particle comes to an abrupt halt for a Péclet number higher than 27. This is attributed to the higher growth rates of second hydrodynamic instability mode, also referred to as quadrupolar instability (Hokmabad *et al.* 2021). This regime is referred to as the stirring regime because the particle surface activity only stirs the fluid around it while the particle is not moving. Although the propulsion characteristics of the particle in the quiescent regime and the stirring regime are similar where the particle is stationary in both cases, the difference between the two cases is clearly evident from the stresslet associated with the particle in these two regimes, as shown in figure 3(*b*). The stresslet in the quiescent regime remains negligible, whereas it is significantly higher in the stirring regime, with the transition from self-propulsion to stirring regime being marked by a sudden increase in the magnitude of the stresslet, and thereby a sudden change in the effective viscosity of the fluid. At higher values of the Péclet number ($\geqslant 55$), a chaotic motion of the particle is observed, and the flow regime is referred to as the chaotic regime (Hu *et al.* 2019, 2022; Kailasham & Khair

https://doi.org/10.1017/jfm.2025.232 Published online by Cambridge University Press

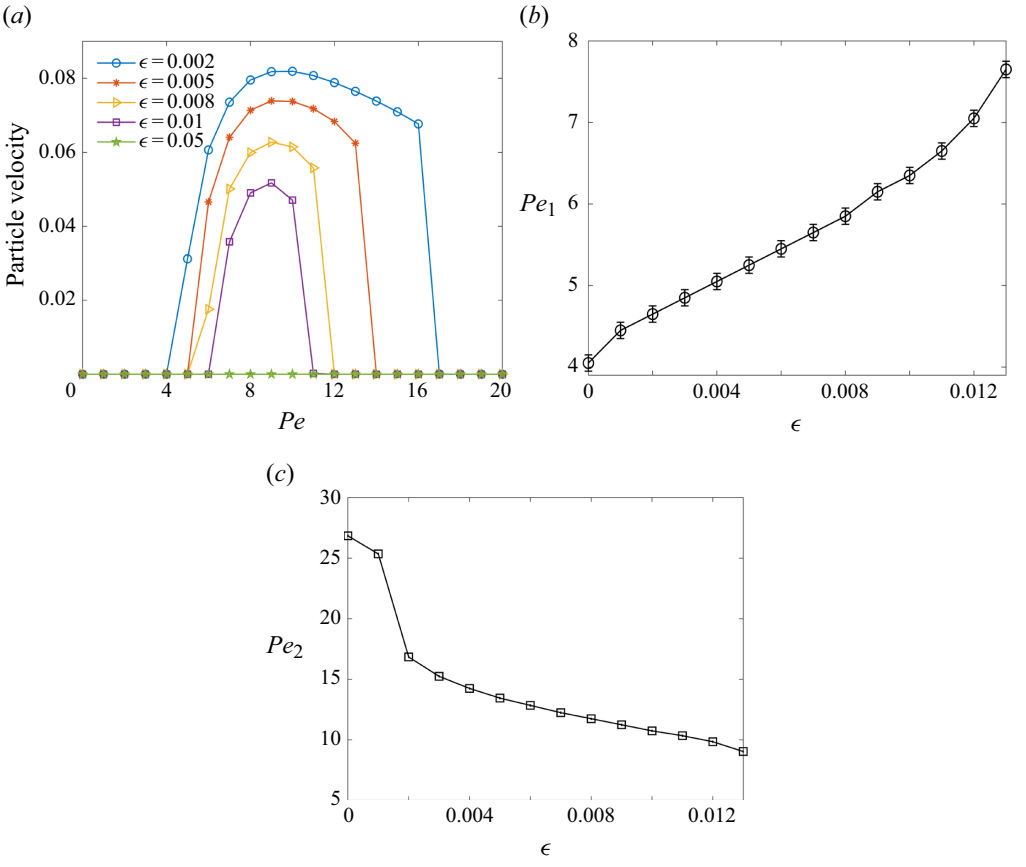


Figure 4. (*a*) The variation of numerically obtained particle velocity with Péclet number for varying strengths of imposed extensional flow. (*a*) The onset of particle self-propulsion and abrupt halt at different values of Pe for varying strengths of imposed extensional flow. (*b*) The change in critical Péclet number for the onset of self-propulsion (Pe_1) with increasing value of imposed strain rate. The self-propulsion in the case of a greater value of imposed strain rate starts much later than the weak imposed extensional flow condition. (*c*) The particle comes to an abrupt halt at a lower Péclet number (Pe_2) for increased strength of imposed extensional flow. The particle is assumed to be stationary if the numerical value of particle velocity is less than 5×10^{-3} (Picella & Michelin 2022).

2022). Note that similar regimes are also reported for chemically active droplets driven by the Marangoni and/or diffusiophoresis effect (Morozov & Michelin 2019*a*; Li 2022; Wang, Zheng & Li 2024).

3.2. *Motion with background uniaxial extensional flow*

Figure 4 illustrates the influence of imposed uniaxial extensional flow on active particle motion, where ϵ represents the relative strength of imposed flow to the self-induced diffusiophoretic slip. As shown in figure 4(*a*), two distinct behaviours emerge, depending on ϵ. For $0 < \epsilon \leqslant 0.013$, the particle motion resembles that in a quiescent medium, while for $\epsilon = 0.05$, the dynamics aligns with passive particles under extensional flow. To analyse coupled effects of surface activity, mobility and imposed flow, the study considers ϵ in the range $0.001-0.05$.

Self-propulsion begins once the Péclet number (Pe) surpasses a critical threshold (Pe_1), but the imposed flow delays this onset as its strength increases, as shown in figure 4(*b*).

https://doi.org/10.1017/jfm.2025.232 Published online by Cambridge University Press

Additionally, higher ϵ causes an earlier transition from self-propulsion to a stirring regime, indicated by an abrupt drop in velocity at a lower Pe (Pe_2), as seen in figure 4(c). For $\epsilon = 0.05$, the imposed flow completely inhibits self-propulsion, rendering the particle stationary even at high Pe. Within $Pe_1 < Pe < Pe_2$ and $\epsilon \leqslant 0.013$, the imposed flow further reduces particle velocity, as shown in figure 4(a).

The imposed extensional flow induces non-uniform solute distribution near the particle, enhancing diffusiophoretic slip. However, the symmetry of uniaxial flow promotes a quadrupolar solute distribution, as depicted in figure 5(e), inhibiting dipolar instabilities required for self-propulsion. Consequently, particle dynamics depend on two parameters: (i) Péclet number (Pe), indicating solute advection strength relative to diffusion, and (ii) strain rate (ϵ), representing imposed flow strength relative to diffusiophoretic slip. Self-propulsion does not begin before $Pe = 4$ for any ϵ because advection is insufficient to overcome diffusion. As ϵ increases, stronger diffusiophoretic slip is needed to counteract the quadrupolar symmetry, delaying self-propulsion onset and increasing Pe_1. This delay is evident for moderate ϵ ($0.001 \leqslant \epsilon \leqslant 0.013$), as shown in figures 4(a) and 4(b).

The transition from self-propulsion to the stirring regime corresponds to the dominance of quadrupolar instability, associated with second-order effects (Chen *et al.* 2021; Hokmabad *et al.* 2021; Kailasham & Khair 2022). The flow field in the stirring regime resembles uniaxial extensional flow, also called the extensile pumping regime (Morozov & Michelin 2019*a*; Kailasham & Khair 2022). While uniaxial flow suppresses dipolar instability, it promotes quadrupolar instability due to its symmetry, as reflected in figures 4(a) and 4(c). Increasing ϵ causes an earlier cessation of self-propulsion at lower Pe_2, leading to an early transition to the stirring regime. For $\epsilon = 0.05$, self-propulsion is completely inhibited, and particle dynamics is dominated by the imposed flow, as the effects of diffusiophoretic slip on particle propulsion become negligible. A similar suppression of self-propulsion under imposed shear flow was observed for disk-shaped particles (Kailasham & Khair 2023*b*). It is important to note that although diffusiophoretic slip at $\epsilon = 0.05$ does not significantly influence the particle's motion, it still affects the overall dynamics and the stresslet associated with the particle, as will be discussed in the following paragraphs.

So far, the impact of imposed flow on active particle motion has been discussed. However, the presence of a particle in any fluid medium modulates the overall rheology of the fluid as well. To investigate the impact of active particle locomotion in imposed extensional flow on the fluid rheology, it is imperative to focus on the solute cloud distribution over the particle surface. The steady-state solute concentration distribution on the particle surface can be expressed in terms of Legendre polynomials as $C|_{r=1} = \sum_{n=0}^{\infty} C_n\, P_n(\eta)$. The relevant modes, C_1 and C_2, can be determined using the orthogonality property of the Legendre polynomials. These modes respectively contribute to the particle self-propulsion and stresslet. This is depicted in figure 5. As discussed earlier, for strong imposed extensional flow ($\epsilon > 0.013$), the extensional flow around the particle tends to strengthen the second mode while simultaneously weakening the first instability mode. As a consequence, the symmetry breaking is not achieved, and the particle remains stationary. Although the particle surface activity and mobility are not able to surpass the effect of strong imposed flow to initiate particle self-propulsion, they do, however, influence the suspension rheology with increase in Pe. For $Pe = 0$, the rheology is governed solely by the imposed extensional flow, which tends to stretch the particle while inducing a positive stresslet and an increased effective viscosity. As Pe increases, the coupled effect of activity and mobility induces an active stresslet having a tendency to oppose the imposed flow condition. This is indicated by a reduction in the stresslet with increase in Pe. In addition to this, the impact of imposed extensional flow

https://doi.org/10.1017/jfm.2025.232 Published online by Cambridge University Press

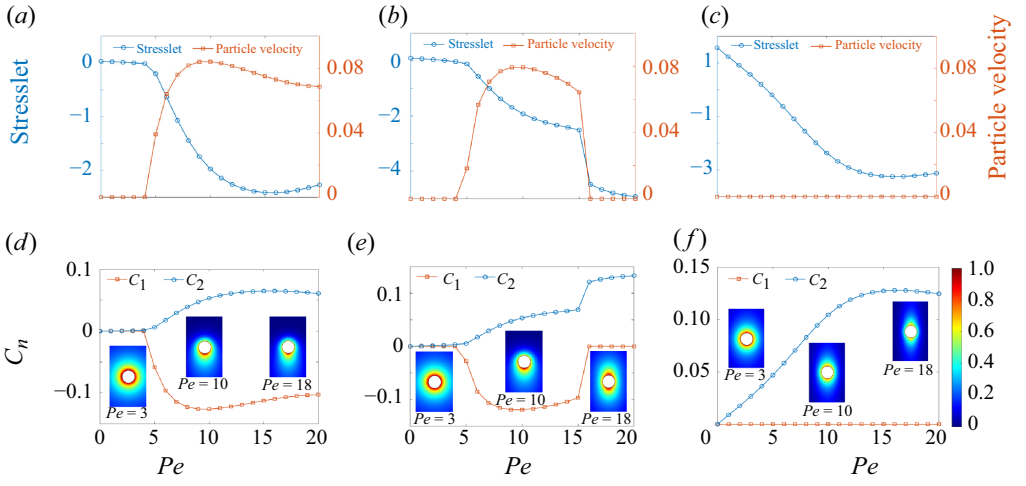


Figure 5. Numerically obtained particle velocity and the induced stresslet along with the solute concentration distribution (C) at the particle surface for (a,d) $\epsilon = 0.001$, (b,e) $\epsilon = 0.003$, and (c,f) $\epsilon = 0.05$. The first mode of solute concentration C_1 represents the asymmetric solute cloud distribution, while the second mode C_2 represents the symmetric solute distribution about the particle surface. For $\epsilon = 0.003$, the abrupt halt in particle motion is characterised with a sudden drop in C_1 and a sudden rise in C_2, whereas for $\epsilon = 0.05$, the self-propulsion does not start, which is represented by $C_1 = 0$.

in enhancing the second mode of solute concentration distribution (C_2) increases. This results in augmentation of the active stresslet (negative) with rise in Pe.

When the strength of the imposed extensional flow is reduced, the impact of self-generated diffusiophoretic slip due to particle surface activity and mobility becomes more noticeable. As mentioned earlier, the activity on the particle's surface in tandem with mobility causes an uneven distribution of solute concentration resulting in the diffusiophoretic slip. This is characterised by an increase in the value of C_1, which in turn causes the particle self-propulsion, as seen in figure 5. Figure 5 indicates that the relative magnitude of the two modes, C_1 and C_2, dictates the magnitude of the stresslet. In the case of weak and intermediate strength of extensional flow ($\epsilon \leqslant 0.013$), the solute concentration distribution achieves dipolar asymmetry at Pe_1, resulting in the self-propulsion of the particle. This is characterised by a higher value of C_1 compared to C_2, resulting in a reduction in the magnitude of the stresslet. This is because the disturbance in the fluid medium near the particle, which is induced as a reaction to self-propulsion, tends to aid the background flow, thereby reducing the opposing effect of surface activity and mobility (characterised by C_2). This results in a reduction in the magnitude of the net stresslet induced by the particle as ϵ decreases. This is depicted in figure 6, where the magnitude of the stresslet for $Pe_1 \leqslant Pe \leqslant Pe_2$ reduces with decrease in ϵ.

As discussed earlier, for dimensionless strain rates ranging from 0.001 to 0.05, the self-propulsion caused by the onset of the first-order dipolar instability mode abruptly stops at a certain Péclet number (Pe_2), owing to the early initiation of higher-order quadrupolar instability, resulting in a symmetric distribution of solute particles that is further enhanced by the imposed extensional flow. This abrupt cessation of propulsion results in the particle entering a state of symmetric extensile pumping, also referred to as a stirring regime. In this condition, the activity of the particle induces stirring of the surrounding fluid (Morozov & Michelin 2019*a*; Kailasham & Khair 2022), with no self-propulsion. The stirring effects act in tandem with the negative active stresslet leading to a sharp rise

https://doi.org/10.1017/jfm.2025.232 Published online by Cambridge University Press

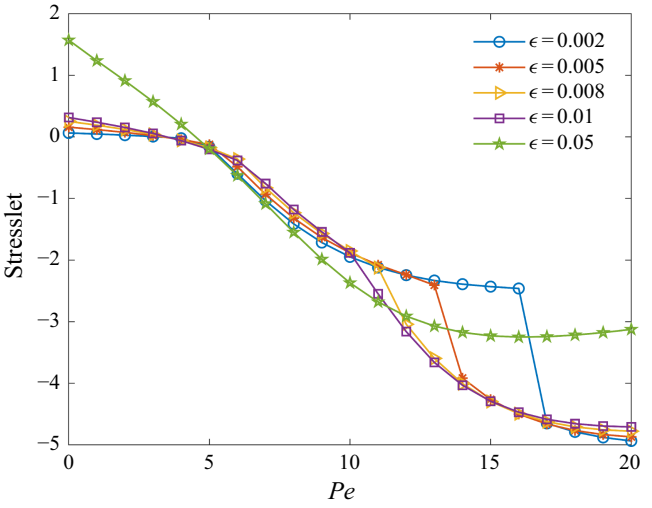


Figure 6. The variation of numerically obtained stresslet with Péclet number for different strengths of imposed extensional flow.

in the net negative stresslet (figure 6), which in turn decreases the effective viscosity of the suspension. This is also characterised by a sudden jump in C_2 and a simultaneous drop in C_1, as depicted in figure 5. The sudden jump in the magnitude of the stresslet results in an abrupt change in the effective viscosity of the fluid. Thus, depending upon the strength of the imposed extensional flow, the coupled effect of imposed extensional flow and the self-induced diffusiophoretic slip can modify the rheological behaviour with increasing Péclet number. A similar increase/decrease in stresslet for active suspension of particles, including bacterial suspension, has been reported in the case of imposed shear flow (Saintillan 2010, 2018; Koch & Subramanian 2011; Frankel & Khair 2014; Kailasham & Khair 2023*b*).

Similar to the case of active particle motion in a quiescent medium, the active particle motion and its subsequent impact on the suspension rheology, when subjected to a uniaxial extensional flow, can be summarised through the regime plot as depicted in figure 7. Although the regimes are similar to that of active particle motion in a quiescent medium, the span and distribution with respect to the strength of imposed flow and Péclet number are different. Additionally, it is observed that with increasing ϵ, both the critical Péclet numbers (Pe_1 and Pe_2) tend to merge together, as depicted in figure 7, resulting in a direct transition to the stirring regime. All this is summarised as follows.

(i) Quiescent regime. This indicates that the self-propulsion has not started or the first-order instability mode has not been attained. Usually, for an active particle in the absence of any imposed flow, this happens when the Péclet number is less than 4. In the presence of extensional flow, the self-propulsion initiates only after a threshold value of the Péclet number (Pe_1), which depends on the magnitude of the imposed strain rate, is attained. The increased strength of imposed extensional flow, i.e. $\epsilon > 0.013$, also results in non-attainment of the first-order instability mode. This is because of the dominance of the imposed uniaxial extensional flow over the self-propelling nature of the diffusiophoretic slip. Although the uniaxial extensional flow tries to make the solute cloud non-uniform, it promotes the quadrupolar

https://doi.org/10.1017/jfm.2025.232 Published online by Cambridge University Press

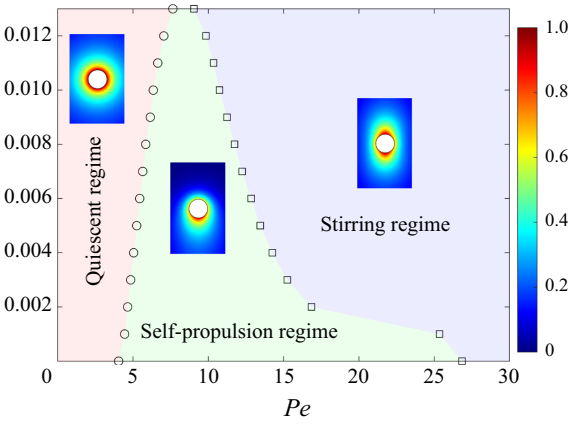


Figure 7. Regimes corresponding to contrasting particle behaviour depending on the Péclet number and strength of imposed uniaxial extensional flow. The quiescent regime signifies that the particle has not started moving. The onset of the self-propulsion regime and end of the quiescent regime is characterised by Pe_1 (circular marker). The abrupt halt of the particle is denoted by the stirring regime. The transition from self-propulsion to the stirring regime is characterised by Pe_2 (rectangular marker). The data are obtained through numerical simulations.

symmetry associated with C_2. This quadrupolar symmetry in solute does not result in self-propulsion as self-propulsion is governed solely by the C_1 mode of solute concentration. Thus for $\epsilon > 0.013$, the self-propulsion regime is not observed with a direct transition from the quiescent regime to the stirring regime.

(ii) Self-propulsion regime. Once the magnitude of self-generated diffusiophoretic slip is strong enough to counter the homogenising effect of diffusion as well as the tendency of the imposed flow to attain quadrupolar symmetry of the solute cloud, an asymmetry in the solute cloud distribution around the particle surface results in its self-propulsion. The regime starts when the Péclet number is greater than the threshold Péclet number (Pe_1). For weak imposed extensional flow, i.e. $\epsilon < 0.001$, the self-propulsion regime continues until $Pe \approx 27$, whereas for intermediate strength of the imposed extensional flow, i.e. $0.001 \leqslant \epsilon \leqslant 0.013$, the propulsion regime is limited to a critical value of the Péclet number (Pe_2), which reduces with increasing strength of imposed flow. Thus an increase in imposed flow strength facilitates an early attainment of the stirring regime.

(iii) Stirring regime. Here, the higher-order quadrupolar instability mode dominates the dipolar propulsion instability mode. This results in the particle coming to a sudden halt. The stirring effect adds to the passive flow-induced stresslet, resulting in an abrupt increase in the net negative stresslet, thereby reducing the effective viscosity of the suspension.

4. Conclusions

The present study investigates the effects of the interaction between particle surface activity and mobility with the applied uniaxial extensional flow on the propulsion behaviour of the particle and its impact on the overall rheology of the suspension. The diffusiophoretic slip induced by the non-uniform solute concentration on the particle surface, when enhanced by the advection, results in self-propulsion of the particle, whereas the imposed uniaxial extensional flow tends to curtail the self-propulsion characteristics. The dynamics of the particle in this coupled system is governed by two parameters,

https://doi.org/10.1017/jfm.2025.232 Published online by Cambridge University Press

namely (i) Péclet number (Pe), denoting the strength of solute advection with respect to diffusion, and (ii) dimensionless strain rate ϵ, which represents the strength of imposed flow relative to the self-induced diffusiophoretic slip. The imposed extensional flow is observed to enhance the non-uniformity in solute concentration distribution in such a way that it promotes quadrupolar symmetry in concentration distribution around the particle surface, suppressing the active particle's self-propulsion. For an intermediate strength of the imposed uniaxial extensional flow, i.e. $0.001 \leqslant \epsilon \leqslant 0.013$, the self-propulsion of the particle starts only after a critical value of the Péclet number (Pe_1), which in turn depends on the imposed strain rate. The Pe_1 value is higher for the greater value of imposed strain rate; i.e. with increasing strength of the imposed extensional flow, the onset of self-propulsion with respect to Péclet number is delayed. In the self-propulsion regime, the magnitude of particle velocity decreases with an increase in ϵ, again showcasing the propulsion-prohibiting tendency of the imposed extensional flow. The particle is also observed to come to an abrupt halt at a relatively lower Péclet number (Pe_2) compared to the case of no external flow. With increasing Pe, the extensile nature of the imposed flow augments the active stresslet (negative) by promoting the quadrupolar second-order symmetry. Additionally, the stirring effect caused by the particle activity post the abrupt halt, i.e. $Pe \geqslant Pe_2$, acts in tandem with the imposed flow condition, thereby reducing the effective viscosity of the suspension. These results could have potential implications in various fields connected to the study of the flow behaviour of suspensions, including moving particles, droplets, and living organisms that exhibit wriggling motion. The present single-particle analysis could be extended to explore the collective dynamics of multi-particle systems in the future, which will be an intriguing field of investigation.

4.1. *Challenges and future directions*

The present analysis is based on a two-dimensional axisymmetric assumption, which holds true as long as the particle remains at the stagnation point of the extensional flow. However, once self-propulsion begins, the particle moves away from the stagnation point, making the problem inherently three-dimensional. Additionally, theoretical studies such as those by Morozov & Michelin (2019*a*), Saha *et al.* (2021), Schnitzer (2023) and Peng & Schnitzer (2023) provide valuable insights into bifurcation analysis and asymmetric modes related to self-propulsion. These works suggest that a bifurcation analysis, especially for $Pe > 4$, could unveil further details about self-propulsion dynamics, and represents a significant avenue for future theoretical exploration. Moreover, the assumption of fore–aft symmetry in our perturbation analysis is valid only up to $Pe = 4$. Beyond this threshold, self-propulsion instabilities render the analysis less applicable. This limitation, coupled with the agreement between the stresslet predictions and numerical results only up to $Pe \sim 4$, as shown in figure 2, underscores the restricted applicability of our perturbation analysis at higher Pe. Therefore, extending the theoretical framework to include stability analysis of the fully three-dimensional model would offer deeper insights into particle dynamics at higher Pe values, and represent a promising direction for future research. In this regard, the solution methodology suggested by Schnitzer (2023) and Peng & Schnitzer (2023) could be applied to analyse the bifurcation at $Pe = 4$ for the resulting three-dimensional unsteady problem.

Acknowledgements. The authors thank Indian Science Technology and Engineering Facilities Map (I-STEM), a programme supported by the Office of the Principal Scientific Adviser to the Government of India, for enabling access to the COMSOL Multiphysics 6.0 software used to carry out the numerical simulations. The authors thank S. Sarkar for verifying the numerical simulation results using the Legendre polynomial expansion method.

https://doi.org/10.1017/jfm.2025.232 Published online by Cambridge University Press

Funding. S.M. gratefully acknowledges support from DST-SERB grant no. EEQ/2021/000561. R.R. gratefully acknowledges the financial support from an IoE postdoctoral research grant of the Indian Institute of Science, Bengaluru, and an NPDF research grant from DST-SERB file no. PDF/2023/000421.

Declaration of interests. The authors declare no conflict of interest.

References

BATCHELOR, G.K. 1970 The stress system in a suspension of force-free particles. *J. Fluid Mech.* **41** (3), 545–570.

BROSSEAU, Q., USABIAGA, F.B., LUSHI, E., WU, Y., RISTROPH, L., ZHANG, J., WARD, M. & SHELLEY, M.J. 2019 Relating rheotaxis and hydrodynamic actuation using asymmetric gold–platinum phoretic rods. *Phys. Rev. Lett.* **123** (17), 178004.

CHEN, X., ZHOU, C. & WANG, W. 2019 Colloidal motors 101: a beginner's guide to colloidal motor research. *Chem. Asian J.* **14** (14), 2388–2405.

CHEN, Y., CHONG, K.L., LIU, H., VERZICCO, R. & LOHSE, D. 2024 Buoyancy-driven attraction of active droplets. *J. Fluid Mech.* **980**, A54.

CHEN, Y., CHONG, K.L., LIU, L., VERZICCO, R. & LOHSE, D. 2021 Instabilities driven by diffusiophoretic flow on catalytic surfaces. *J. Fluid Mech.* **919**, A10.

DESAI, N. & MICHELIN, S. 2021 Instability and self-propulsion of active droplets along a wall. *Phys. Rev. Fluids* **6** (11), 114103.

EBBENS, S.J. & HOWSE, J.R. 2010 In pursuit of propulsion at the nanoscale. *Soft Matter* **6** (4), 726–738.

FARUTIN, A., RIZVI, S.M., HU, W.-F., LIN, T.-S., RAFAI, S. & MISBAH, C. 2023 Motility and swimming: universal description and generic trajectories. *Eur. Phys. J. E* **46** (12), 1–20.

FRANKEL, A.E. & KHAIR, A.S. 2014 Dynamics of a self-diffusiophoretic particle in shear flow. *Phys. Rev. E* **90** (1), 013030.

GOLESTANIAN, R., LIVERPOOL, T.B. & AJDARI, A. 2007 Designing phoretic micro- and nano-swimmers. *New J. Phys.* **9** (5), 126.

HOKMABAD, B.V., DEY, R., JALAAL, M., MOHANTY, D., ALMUKAMBETOVA, M., BALDWIN, K.A., LOHSE, D. & MAASS, C.C. 2021 Emergence of bimodal motility in active droplets. *Phys. Rev. X* **11** (1), 011043.

HOWSE, J.R., JONES, R.A.L., RYAN, A.J., GOUGH, T., VAFABAKHSH, R. & GOLESTANIAN, R. 2007 Self-motile colloidal particles: from directed propulsion to random walk. *Phys. Rev. Lett.* **99** (4), 048102.

HU, W.-F., LIN, T.-S., RAFAI, S. & MISBAH, C. 2019 Chaotic swimming of phoretic particles. *Phys. Rev. Lett.* **123** (23), 238004.

HU, W.-F., LIN, T.-S., RAFAI, S. & MISBAH, C. 2022 Spontaneous locomotion of phoretic particles in three dimensions. *Phys. Rev. Fluids* **7** (3), 034003.

ILLIEN, P., GOLESTANIAN, R. & SEN, A. 2017 'Fuelled' motion: phoretic motility and collective behaviour of active colloids. *Chem. Soc. Rev.* **46** (18), 5508–5518.

IZRI, Z., VAN DER LINDEN, M.N., MICHELIN, S. & DAUCHOT, O. 2014 Self-propulsion of pure water droplets by spontaneous Marangoni-stress-driven motion. *Phys. Rev. Lett.* **113** (24), 248302.

KAILASHAM, R. & KHAIR, A.S. 2022 Dynamics of forced and unforced autophoretic particles. *J. Fluid Mech.* **948**, A41.

KAILASHAM, R. & KHAIR, A.S. 2023*a* Effect of speed fluctuations on the collective dynamics of active disks. *Soft Matter* **19** (40), 7764–7774.

KAILASHAM, R. & KHAIR, A.S. 2023*b* Non-Brownian diffusion and chaotic rheology of autophoretic disks. *Phys. Rev. E* **107** (4), 044609.

KATURI, J., USPAL, W.E., SIMMCHEN, J., MIGUEL-LÓPEZ, A. & SÁNCHEZ, S. 2018 Cross-stream migration of active particles. *Sci. Adv.* **4** (1), eaao1755.

KOCH, D.L. & SUBRAMANIAN, G. 2011 Collective hydrodynamics of swimming microorganisms: living fluids. *Annu. Rev. Fluid Mech.* **43** (1), 637–659.

LAUGA, E. & MICHELIN, S. 2016 Stresslets induced by active swimmers. *Phys. Rev. Lett.* **117** (14), 148001.

LEAL, L.G. 2007 *Advanced Transport Phenomena: Fluid Mechanics and Convective Transport Processes*. Cambridge Series in Chemical Engineering, vol. **7**. Cambridge University Press.

LI, G. 2022 Swimming dynamics of a self-propelled droplet. *J. Fluid Mech.* **934**, A20.

LIN, C.-J., PEERY, J.H. & SCHOWALTER, W.R. 1970 Simple shear flow round a rigid sphere: inertial effects and suspension rheology. *J. Fluid Mech.* **44** (1), 1–17.

MAASS, C.C., KRÜGER, C., HERMINGHAUS, S. & BAHR, C. 2016 Swimming droplets. *Annu. Rev. Condens. Matter Phys.* **7** (1), 171–193.

https://doi.org/10.1017/jfm.2025.232 Published online by Cambridge University Press

MANDAL, S., SINHA, S., BANDOPADHYAY, A. & CHAKRABORTY, S. 2018 Drop deformation and emulsion rheology under the combined influence of uniform electric field and linear flow. *J. Fluid Mech.* **841**, 408–433.

MCDONNELL, A.G., GOPESH, T.C., LO, J., O'BRYAN, M., YEO, L.Y., FRIEND, J.R. & PRABHAKAR, R. 2015 Motility induced changes in viscosity of suspensions of swimming microbes in extensional flows. *Soft Matter* **11** (23), 4658–4668.

MICHELIN, S. 2023 Self-propulsion of chemically active droplets. *Annu. Rev. Fluid Mech.* **55** (1), 77–101.

MICHELIN, S. & LAUGA, E. 2014 Phoretic self-propulsion at finite Péclet numbers. *J. Fluid Mech.* **747**, 572–604.

MICHELIN, S., LAUGA, E. & BARTOLO, D. 2013 Spontaneous autophoretic motion of isotropic particles. *Phys. Fluids* **25** (6), 061701.

MORAN, J.L. & POSNER, J.D. 2017 Phoretic self-propulsion. *Annu. Rev. Fluid Mech.* **49** (1), 511–540.

MOROZOV M. & MICHELIN S. 2019*a* Nonlinear dynamics of a chemically-active drop: from steady to chaotic self-propulsion. *J. Chem. Phys.* **150** (4), 044110.

MOROZOV, M. & MICHELIN, S. 2019*b* Self-propulsion near the onset of Marangoni instability of deformable active droplets. *J. Fluid Mech.* **860**, 711–738.

PENG, G.G. & SCHNITZER, O. 2023 Weakly nonlinear dynamics of a chemically active particle near the threshold for spontaneous motion. II. History-dependent motion. *Phys. Rev. Fluids* **8** (3), 033602.

PICELLA, F. & MICHELIN, S. 2022 Confined self-propulsion of an isotropic active colloid. *J. Fluid Mech.* **933**, A27.

POPESCU, M.N. 2020 Chemically active particles: from one to few on the way to many. *Langmuir* **36** (25), 6861–6870.

RAJA, R.V., SUBRAMANIAN, G. & KOCH, D.L. 2010 Inertial effects on the rheology of a dilute emulsion. *J. Fluid Mech.* **646**, 255–296.

RAMASWAMY, S. 2010 The mechanics and statistics of active matter. *Annu. Rev. Condens. Matter Phys.* **1** (1), 323–345.

SAHA, S. & YARIV, E. 2022 Phoretic self-propulsion of a slightly inhomogeneous disc. *J. Fluid Mech.* **940**, A24.

SAHA, S., YARIV, E. & SCHNITZER, O. 2021 Isotropically active colloids under uniform force fields: from forced to spontaneous motion. *J. Fluid Mech.* **916**, A47.

SAINTILLAN, D. 2010 The dilute rheology of swimming suspensions: a simple kinetic model. *Exp. Mech.* **50** (9), 1275–1281.

SAINTILLAN, D. 2018 Rheology of active fluids. *Annu. Rev. Fluid Mech.* **50** (1), 563–592.

SCHNITZER, O. 2023 Weakly nonlinear dynamics of a chemically active particle near the threshold for spontaneous motion. I. Adjoint method. *Phys. Rev. Fluids* **8** (3), 034201.

SEEMANN, R., FLEURY, J.-B. & MAASS, C.C. 2016 Self-propelled droplets. *Eur. Phys. J. Special Topics* **225** (11–12), 2227–2240.

SHARAN, P., XIAO, Z., MANCUSO, V., USPAL, W.E. & SIMMCHEN, J. 2022 Upstream rheotaxis of catalytic Janus spheres. *ACS Nano* **16** (3), 4599–4608.

SHREEKRISHNA, S., MANDAL, S. & DAS, S. 2024 Spontaneous emergence of motion of an isotropic active particle in a Carreau fluid. *Soft Matter* **20** (48), 9683–9693.

SI, B.R., PATEL, P. & MANGAL, R. 2020 Self-propelled Janus colloids in shear flow. *Langmuir* **36** (40), 11888–11898.

STARK, H. 2016 Swimming in external fields. *Eur. Phys. J. Special Topics* **225** (11–12), 2369–2387.

SUBRAMANIAN, G., KOCH, D.L., ZHANG, J. & YANG, C. 2011 The influence of the inertially dominated outer region on the rheology of a dilute dispersion of low-Reynolds-number drops or rigid particles. *J. Fluid Mech.* **674**, 307–358.

TAYLOR, G.I. 1932 The viscosity of a fluid containing small drops of another fluid. *Proc. R. Soc. Lond. A* **138** (834), 41–48.

TEN HAGEN, B., KÜMMEL, F., WITTKOWSKI, R., TAKAGI, D., LÖWEN, H. & BECHINGER, C. 2014 Gravitaxis of asymmetric self-propelled colloidal particles. *Nat. Commun.* **5** (1), 4829.

USPAL, W.E., POPESCU, M.N., DIETRICH, S. & TASINKEVYCH, M. 2015 Rheotaxis of spherical active particles near a planar wall. *Soft Matter* **11** (33), 6613–6632.

WANG, J. 2013 *Nanomachines: Fundamentals and Applications*. John Wiley & Sons.

WANG, Y., ZHENG, L. & LI, G. 2024 Self-propulsion of a droplet induced by combined diffusiophoresis and marangoni effects. *Electrophoresis*. https://doi.org/10.1002/elps.202400005.

WIRTZ, D. 2009 Particle-tracking microrheology of living cells: principles and applications. *Annu. Rev. Biophys.* **38** (1), 301–326.

YANG, Q., JIANG, M., PICANO, F. & ZHU, L. 2024 Shaping active matter from crystalline solids to active turbulence. *Nat. Commun.* **15** (1), 2874.

https://doi.org/10.1017/jfm.2025.232 Published online by Cambridge University Press

YARIV, E. & KAYNAN, U. 2017 Phoretic drag reduction of chemically active homogeneous spheres under force fields and shear flows. *Phys. Rev. Fluids* **2** (1), 012201.
ZHAO, G. & PUMERA, M. 2012 Macroscopic self-propelled objects. *Chem. Asian J.* **7** (9), 1994–2002.
ZHU, G. & ZHU, L. 2023 Self-propulsion of an elliptical phoretic disk emitting solute uniformly. *J. Fluid Mech.* **974**, A57.
ZÖTTL, A. & STARK, H. 2016 Emergent behavior in active colloids. *J. Phys.: Condens. Matter* **28** (25), 253001.

https://doi.org/10.1017/jfm.2025.232 Published online by Cambridge University Press